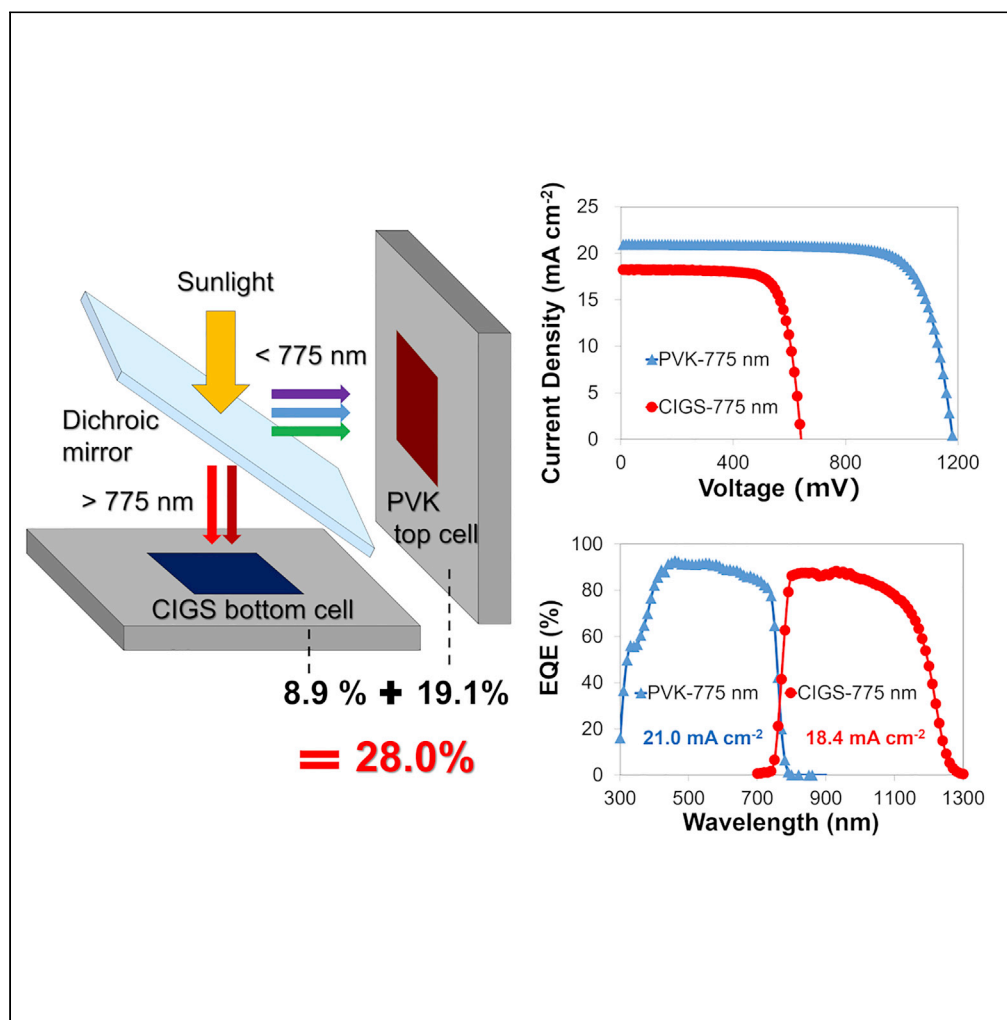**Article**

Perovskite/CIGS Spectral Splitting Double Junction Solar Cell with 28% Power Conversion Efficiency

Motoshi Nakamura, Keishi Tada, Takumi Kinoshita, ..., Yuta Higashino, Hiroki Sugimoto, Hiroshi Segawa

csegawa@mail.ecc.u-tokyo.ac.jp

HIGHLIGHTS

CIGS bottom solar cells with E_g ranging from 1.02 to 1.14 eV are prepared

The lower the E_g of CIGS bottom cell, the higher PCE of PVK/CIGS tandem solar cell

PCE of 28% was demonstrated in a 1 cm^2-sized PVK/CIGS 4-Terminal solar cell

The result can be utilized to design better tandem solar cell in the future

Article

Perovskite/CIGS Spectral Splitting Double Junction Solar Cell with 28% Power Conversion Efficiency

Motoshi Nakamura,[1,2] Keishi Tada,[3] Takumi Kinoshita,[3] Takeru Bessho,[2] Chie Nishiyama,[2] Issei Takenaka,[1] Yoshinori Kimoto,[1] Yuta Higashino,[1] Hiroki Sugimoto,[1] and Hiroshi Segawa[2,3,4,*]

SUMMARY

The highest theoretical efficiency of double junction solar cells is predicted for architectures with the bottom cell bandgap (E_g) of approximately 0.9–1.0 eV, which is lower than that of a typical Si cell (1.1 eV). Cu(In,Ga)(Se,S)$_2$ (CIGS) solar cells exhibit a tunable E_g depending on their elemental composition and depth profile. In this study, various CIGS solar cells with E_g ranging from 1.02 to 1.14 eV are prepared and a spectrum splitting system is used to experimentally demonstrate the effect of using lower-E_g cells as the bottom cell of two-junction solar cells. The four-terminal tandem cell configuration fabricated using a mixed-halide perovskite top cell (E_g = 1.59 eV; stand-alone efficiency = 21.0%) and CIGS bottom cell (E_g = 1.02 eV; stand-alone efficiency = 21.5%) with a 775-nm spectral splitting mirror exhibits an efficiency of 28.0% at the aperture area of 1 cm^2.

INTRODUCTION

Improving the power conversion efficiency (PCE) of solar cells is essential for reducing the solar power cost (Peters et al., 2019). Solar cells with single-junction structures have reached the theoretical limit of PCE, and the possibility of further improvement of PCE is significantly low (Shockley and Queisser, 1961; Green et al., 2020). One of the approaches for overcoming this limitation is the introduction of tandem structures, where two or more solar cells with different bandgaps (E_g) are stacked while optimizing the wavelength absorption range. In this method, depending on the number of cells used, the theoretical PCE limit can be exceeded up to 50% (Meillaud et al., 2006; Alharbi and Kais, 2015). In fact, a PCE of approximately 40% was reported for III-V multi-junction cells (Green et al., 2020). However, the III-V semiconductor-based tandem devices are expensive, which limits their current applications to only a few markets, such as the space industry (Bosi and Pelosi, 2007).

For attaining a high PCE without an excessive cost, double junction devices that are constructed with perovskite (PVK) solar cells as top cells and Si (Chen et al., 2020; Uzu et al., 2015; Duong et al., 2020; Xu et al., 2020; Jaysankar et al., 2019b; Wang et al., 2020), Cu(In,Ga)(Se,S)$_2$ (CIGS) (Kim et al., 2019; Gharibzadeh et al., 2020; Shen et al., 2018; Jiang et al., 2020; Jaysankar et al., 2019a; Al-Ashouri et al., 2019; Han et al., 2018), PVK (Tong et al., 2019; Lin et al., 2019; Palmstrom et al., 2019; Zhao et al., 2018; Yao et al., 2020; Abdollahi Nejand et al., 2020; Yang et al., 2019), and dye-sensitized (DS) (Kinoshita et al., 2015; Hosseinnezhad 2019) solar cells as bottom cells have garnered considerable attention recently. Although a higher PCE has been reported for the PVK/Si combination, the optimal E_g of the bottom cell in the double junction devices ranges from 0.9 to 1.0 eV (see Figure S1), which is lower than the typical E_g of crystalline Si solar cells (1.1 eV). However, depending on their elemental compositions and depth profiles, CIGS solar cells possess a tunable E_g, which can be as low as 1.0 eV (Nakamura et al., 2019), close to the optimal value of the bottom cell for both two-terminal (2-T) and four-terminal (4-T) tandem solar cells. In this study, we experimentally show that the PCE of the double junction solar cells is higher when the bottom cell E_g is closer to 1.0 eV, as predicted by theoretical studies. Subsequently, we conclude that CIGS solar cells are potentially the most superior among the choices as the bottom cell of Perovskite-based double junction solar cells.

RESULTS AND DISCUSSION

The tandem solar cell with a spectral splitting system was constructed using a PVK top cell, CIGS bottom cell, and a dichroic mirror that was fixed at an angle of 45°, as schematically shown in Figure 1.

[1]Advanced Technology Research Laboratories, Idemitsu Kosan Co.,Ltd., 123-1 Shimokawairi, Atsugi, Kanagawa 243-0206, Japan

[2]Research Center for Advanced Science and Technology (RCAST), the University of Tokyo, 4-6-1, Komaba, Meguro-ku, Tokyo 153-8904, Japan

[3]Department of General Systems Studies, Graduate School of Arts and Sciences, the University of Tokyo, 3-8-1 Komaba, Meguro-ku, Tokyo 153-8902, Japan

[4]Lead Contact

*Correspondence: csegawa@mail.ecc.u-tokyo.ac.jp

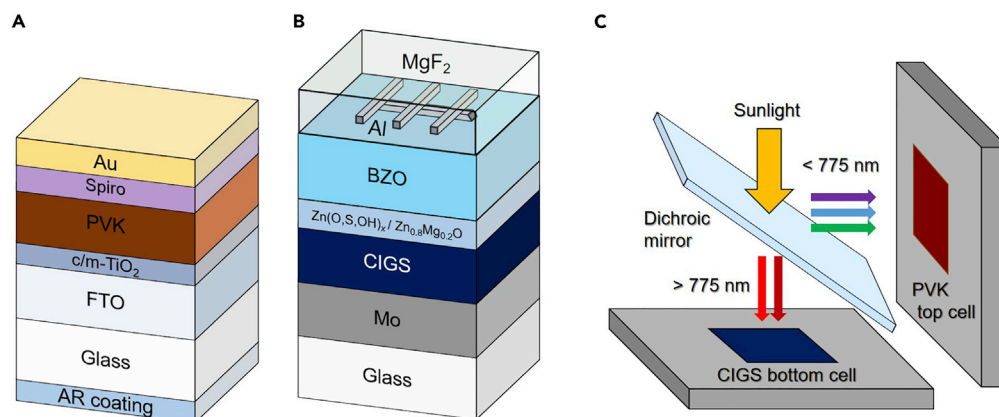https://doi.org/10.1016/j.isci.2020.101817

Figure 1. Schematics of Fabricated Tandem Solar Cells
(A) PVK top cell.
(B) CIGS bottom cell.
(C) Spectrum splitting system with a dichroic mirror.

The layered structure of the fabricated 0.995 cm^2-aperture sized PVK cell was Fluorine-doped tin oxide (FTO)/c-TiO$_2$/m-TiO$_2$/PVK/Spiro-OMeTAD/Au, where the composition of PVK was selected as [K$_{0.05}$(FA$_{0.85}$MA$_{0.15}$)$_{0.95}$]Pb (I$_{0.85}$Br$_{0.15}$)$_3$. The fabrication using mixed halide and alkali metal-doped mixed cation PVK has several advantages, the details of which are described elsewhere (Tang et al., 2017; Lu et al., 2020). However, the main reasons of using the PVK include an increase in the efficiency and reduction of the hysteresis in the current density-voltage (J-V) characteristics. The external quantum efficiency (EQE) spectrum and J-V curve of the fabricated PVK cell measured under the standard 1-sun condition (i.e., without using the dichroic mirror) are shown in Figures 2A and 2B, respectively. The E_g of the PVK cell was determined to be 1.59 eV using the peak position of the first order derivative of the EQE curve (-d(EQE)/dλ) (Krückemeier et al., 2020), which is an ideal value for the top cell of a two-junction tandem solar cell (see Figure S1). The efficiency of the fabricated 1 cm^2-aperture sized PVK cell measured under 1,000 W/ m^2 in the reverse J-V scan was 21.0% with J_{sc}, V_{oc}, and FF of 22.7 mA cm^{-2}, 1,181.8 mV, and 78.1%, respectively. The efficiency of the cell in the forward J-V scan was measured to be 20.3% with J_{sc}, V_{oc}, and FF of 22.6 mA cm^{-2}, 1,173.8 mV, and 76.5%, respectively.

CIGS bottom cells with an aperture area of 1.04 cm^2 were fabricated using the sulfurization after selenization (SAS) process, where a Copper-Gallium/Indium metal precursor on a glass/Molybdenum substrate was selenized with H$_2$Se gas followed by sulfurization with H$_2$S gas in a closed furnace. More than 100 CIGS cells with various E_g values were prepared by adjusting the elemental depth profile of the CIGS absorber layer via tuning some of the parameters in the SAS process, as described in a previous study (Nakamura et al., 2019). Among these cells, four CIGS cells with approximately the same efficiencies (21.5 ± 0.3%) and FFs (75 ± 2%) but with different E_g values ranging from 1.02 to 1.14 eV were used for constructing the tandem structure. The normalized EQE spectra and J-V curves of these four CIGS cells are shown in Figures 2C and 2D, respectively. Unlike PVK cells, CIGS cells generally showed negligible hysteresis; therefore, we displayed the J-V curves in the forward direction only. The device parameters are summarized in Table 1. The elemental depth profiles measured by glow discharge optical emission spectroscopy and calculated E_g depth profiles using an empirical equation are shown in Figure S2 (Bär et al., 2004).

The J-V curves and EQE spectra of the PVK top cell and the CIGS bottom cells measured using the dichroic mirror with splitting wavelength of 775 nm are shown in Figure 3, and the device parameters are summarized in Table 2. The splitting edge wavelength of the dichroic mirror was selected because 775 nm (or 1.60 eV) approximately matches the E_g of the PVK top cell (1.59 eV). The PCE of the PVK cell reduced from 21.0% to 19.1% because of the reduced J_s and FF when the mirror was used. This reduction is reasonable considering that there are parasitic optical losses in the mirror as well as the slight mismatch between the splitting wavelengths and the E_g of the PVK cell. Nevertheless, retaining greater than 90% of the original PCE implies that the spectrum splitting system is well designed with the appropriate choice of wavelength. The PCE of all CIGS bottom cells with different E_g were almost the same when measured without
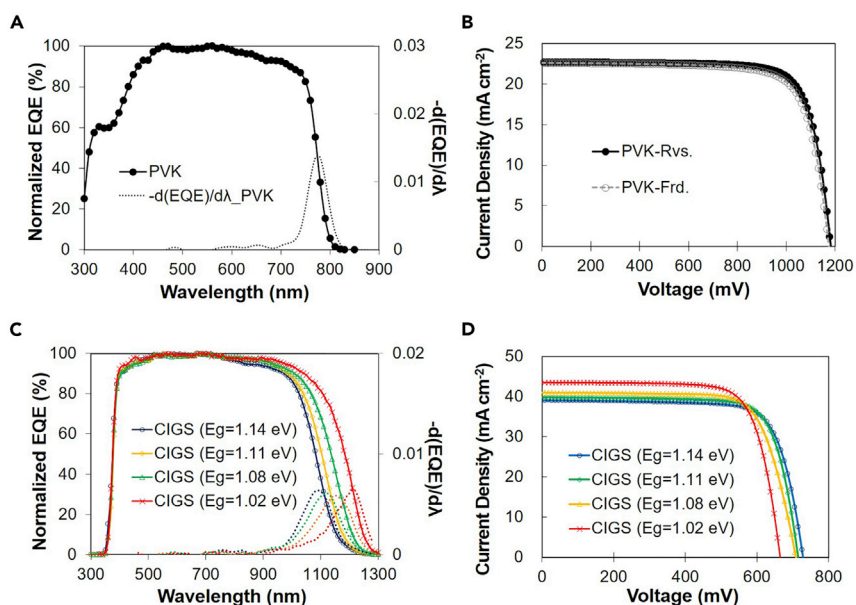
Figure 2. Device Characteristics of the PVK and CIGS Cells Measured Under the Standard 1-sun Irradiation Condition without Using a Dichroic Mirror
(A) Normalized EQE and -d(EQE)/dλ curve of PVK cell.
(B) Forward and reverse scanned *J-V* curves of PVK cell.
(C) EQE and -d(EQE)/dλ curves of CIGS cells.
(D) Forward scanned *J-V* curves of CIGS cells.

the mirror, as shown in Table 1. Moreover, cells with a lower E_g showed a higher efficiency when measured with the mirror. Finally, the PCE difference of the cells with E_g of 1.02 and 1.14 eV reaches as high as 1.4%. This experimental value is in good agreement with the theoretical results, obtained from the detailed balanced calculations shown in Figure 4 (De Vos, 1980). The same trend was observed when the CIGS bottom cells were measured under dichroic mirrors with other splitting wavelengths (see Figure S3). To the best of our knowledge, this is the first report on the experimental procedure and evaluation of the advantage of using low-E_g CIGS as the bottom cell of a tandem device with PVK solar cells.

The overall PCE of the 4-T tandem cell with the spectral splitting system is 28%, comprising the PVK top cell with 19.1% PCE and the lowest-E_g CIGS bottom cell with 8.9% PCE. This is one of the highest reported PCE for the experimentally fabricated PVK-based tandem solar cells (see Table S1).

CONCLUSION

In this study, we experimentally demonstrated that the PCE of a double junction solar cell is higher when the E_g of the bottom cell is closer to 1.0 eV, as predicted theoretically. The device PCE was proven to be increased by an absolute 1.4% when the bottom cell E_g reduced from 1.14 to 1.02 eV. This result indicated

	PCE (%)	J_{sc} (mA cm^{-2})	V_{oc} (mV)	FF (%)
PVK-Rvs.	21.0	22.7	1,181.8	78.1
PVK-Frd.	20.3	22.6	1,173.8	76.5
CIGS (E_g = 1.14 eV)	21.6	39.1	728.8	75.7
CIGS (E_g = 1.11 eV)	21.8	39.8	715.1	76.5
CIGS (E_g = 1.08 eV)	21.5	41.0	708.9	74.1
CIGS (E_g = 1.02 eV)	21.5	43.6	659.0	74.8

Table 1. Parameters of the PVK and CIGS Solar Cells Extracted from the *J-V* Curves and EQE Spectra in Figure 2
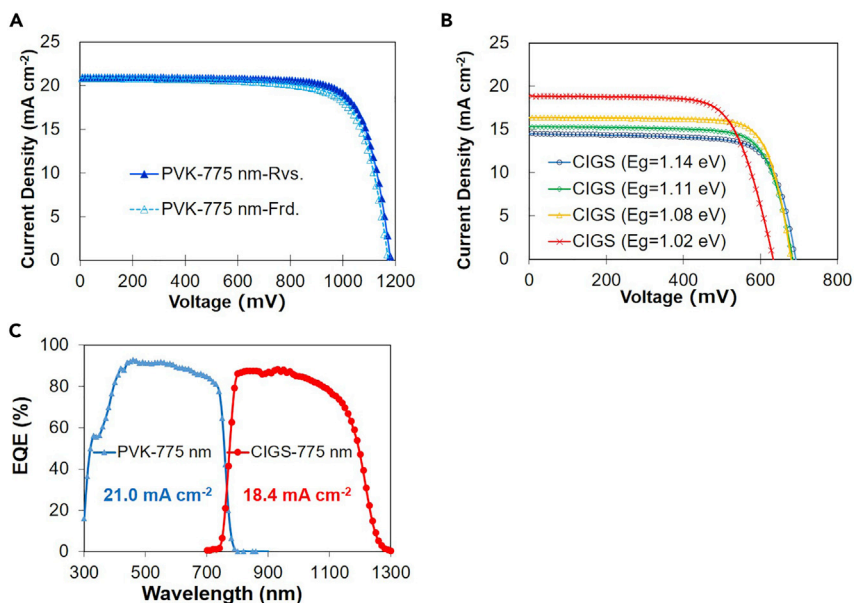
Figure 3. Device Characteristics of the PVK Top Cell and CIGS Bottom Cells Measured in Presence of the Dichroic Mirror with a Splitting Wavelength of 775 nm

(A) Forward and reverse scanned J-V curves of PVK top cell.

(B) J-V curves of CIGS cells with various bandgaps.

(C) EQE of the PVK top cell and CIGS bottom cell with E_g of 1.02 eV.

the potential superiority of PVK/CIGS tandem solar cells over PVK/Si cells because a crystalline Si cell has a fixed E_g of approximately 1.1 eV. A high PCE of 28% was achieved in a PVK/CIGS 4-Terminal double junction structure solar cell comprising a PVK top cell and a CIGS bottom cell with E_g of 1.59 and 1.02 eV, respectively, combined in a spectrum splitting system equipped with a dichroic mirror with splitting wavelengths of 775 nm. As PVK and CIGS are both thin films, tandem devices using these materials can potentially exhibit high flexibilities, which cannot be achieved with Si cells. Spectrum splitting tandem cells may not be ideal for practical applications; however, our study is significantly important because we have shown experimentally that this PVK/CIGS tandem solar cell is not only mechanically superior but also exhibits a higher efficiency compared with Si-based tandem solar cell configurations. These observations will be utilized to design better tandem solar cells in future.

Limitations of the Study

In this study, we did not conduct MPP measurement; therefore, the steady-state efficiency may differ from the values presented in the paper to some extent. To compare the PCEs of the spectrum splitting tandem

	PCE (%)	J_{sc} (mA cm^{-2})	V_{oc} (mV)	FF (%)
PVK-775 nm-Rev.	19.1	21.0	1,182.0	77.2
PVK-775 nm-Frd.	18.3	20.9	1,172.8	74.6
CIGS (Eg = 1.14 eV)	7.5	14.5	690.9	74.9
CIGS (Eg = 1.11 eV)	7.9	15.3	682.7	75.3
CIGS (Eg = 1.08 eV)	8.6	16.3	678.9	77.5
CIGS (Eg = 1.02 eV)	8.9	18.4	637.0	75.8
4-T tandem (best)	28.0	–	–	–

Table 2. Solar Cell Parameters of the PVK Top Cell and CIGS Bottom Cells Extracted from the J-V Curves and EQE Spectra in Figure 3. The highest 4-T tandem cell efficiency was obtained when the CIGS bottom cell with Eg of 1.02 eV was used.
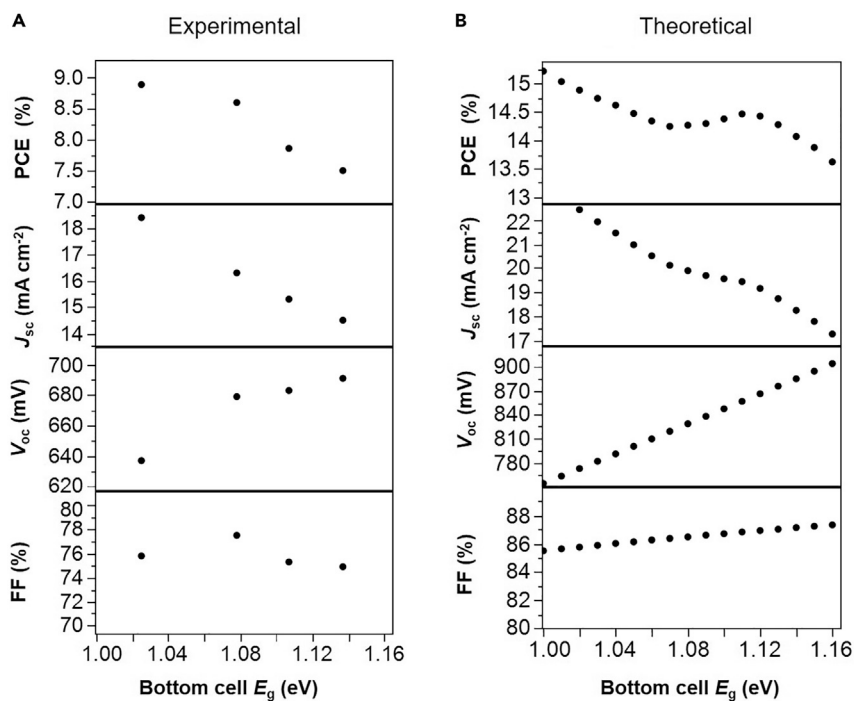
Figure 4. Relation between the Solar Cell Parameters and Bottom Cell E_g

(A) Experimental results for the CIGS bottom cells measured with the dichroic mirror in the spectrum splitting system.

(B) A detailed balanced calculation of the device performance of the bottom cell when the top cell E_g is fixed at 1.6 eV.

devices to other types of tandem devices may not be ideal as most of the optical losses are not taken into consideration for the former; however, the result of this research should provide a guideline for an optimal material design in the fabrication of tandem solar cells in the future.

Resource Availability

Lead Contact

Further information and requests for resources and reagents should be directed to and will be fulfilled by the Lead Contact, Hiroshi Segawa (csegawa@mail.ecc.u-tokyo.ac.jp).

Materials Availability

This study did not generate any new unique reagent.

Data and Code Availability

The data that support the findings of this study are available from the corresponding author upon reasonable request.

METHODS

All methods can be found in the accompanying Transparent Methods supplemental file.

SUPPLEMENTAL INFORMATION

Supplemental Information can be found online at https://doi.org/10.1016/j.isci.2020.101817.

ACKNOWLEDGMENTS

REFERENCES

Abdollahi Nejand, B., Hossain, I.M., Jakoby, M., Moghadamzadeh, S., Abzieher, T., Gharibzadeh, S., Schwenzer, J.A., Nazari, P., Schackmar, F., Hauschild, D., et al. (2020). Vacuum-assisted growth of low-bandgap thin films (FA$_{0.8}$MA$_{0.2}$Sn$_{0.5}$Pb$_{0.5}$I$_3$) for all-perovskite tandem solar cells. Adv. Energy Mater. *10*, 1902583.

Al-Ashouri, A., Magomedov, A., Roß, M., Jošt, M., Talaikis, M., Chistiakova, G., Bertram, T., Márquez, J.A., Köhnen, E., Kasparavičius, E., et al. (2019). Conformal monolayer contacts with lossless interfaces for perovskite single junction and monolithic tandem solar cells. Energy Environ. Sci. *12*, 3356–3369.

Alharbi, F.H., and Kais, S. (2015). Theoretical limits of photovoltaics efficiency and possible improvements by intuitive approaches learned from photosynthesis and quantum coherence. Renew. Sustain. Energy Rev. *43*, 1073–1089.

Bär, M., Bohne, W., Röhrich, J., Strub, E., Lindner, S., Lux-Steiner, M.C., Fischer, C.H., Niesen, T.P., and Karg, F. (2004). Determination of the band gap depth profile of the penternary Cu(In$_{(1-x)}$Ga$_x$)(S$_y$Se$_{(1-y)}$)$_2$ chalcopyrite from its composition gradient. J. Appl. Phys. *96*, 3857–3860.

Bosi, M., and Pelosi, C. (2007). The potential of III-V semiconductors as terrestrial photovoltaic devices. Prog. Photovoltaics Res. Appl. *15*, 51–68.

Chen, B., Baek, S., Hou, Y., Aydin, E., De Bastiani, M., Scheffel, B., Proppe, A., Huang, Z., Wei, M., Wang, Y., et al. (2020). Enhanced optical path and electron diffusion length enable high-efficiency perovskite tandems. Nat. Commun. *11*, 1257.

Duong, T., Pham, H., Kho, T.C., Phang, P., Fong, K.C., Yan, D., Yin, Y., Peng, J., Mahmud, M.A., Gharibzadeh, S., et al. (2020). High efficiency perovskite-silicon tandem solar cells: effect of surface coating versus bulk incorporation of 2D perovskite. Adv. Energy Mater. *10*, 1–15.

Gharibzadeh, S., Hossain, I.M., Fassl, P., Nejand, B.A., Abzieher, T., Schultes, M., Ahlswede, E., Jackson, P., Powalla, M., Schäfer, S., et al. (2020). 2D/3D heterostructure for semitransparent perovskite solar cells with engineered bandgap enables efficiencies exceeding 25% in four-terminal tandems with silicon and CIGS. Adv. Funct. Mater. 1909919.

Green, M.A., Dunlop, E.D., Hohl-Ebinger, J., Yoshita, M., Kopidakis, N., and Hao, X. (2020). Solar cell efficiency tables (version 56). Prog. Photovoltaics Res. Appl. *28*, 629–638.

Han, Q., Hsieh, Y.-T., Meng, L., Wu, J.-L., Sun, P., Yao, E.-P., Chang, S.-Y., Bae, S.-H., Kato, T., Bermudez, V., et al. (2018). High-performance perovskite/Cu(In,Ga)Se$_2$ monolithic tandem solar cells. Science *361*, 904–908.

Hosseinnezhad, M. (2019). Enhanced performance of dye-sensitized solar cells using perovskite/DSSCs tandem design. J. Electron. Mater. *48*, 5403–5408.

Jaysankar, M., Paetel, S., Ahlswede, E., Paetzold, U.W., Aernouts, T., Gehlhaar, R., and Poortmans, J. (2019a). Toward scalable perovskite-based multijunction solar modules. Prog. Photovoltaics Res. Appl. *27*, 733–738.

Jaysankar, M., Raul, B.A.L., Bastos, J., Burgess, C., Weijtens, C., Creatore, M., Aernouts, T., Kuang, Y., Gehlhaar, R., Hadipour, A., et al. (2019b). Minimizing voltage loss in wide-bandgap perovskites for tandem solar cells. ACS Energy Lett. *4*, 259–264.

Jiang, Y., Feurer, T., Carron, R., Torres-sevilla, G., Moser, T., Pisoni, S., Erni, R., Rossell, M.D., Ochoa, M., Hertwig, R., et al. (2020). High mobility In$_2$O$_3$: H electrodes for four- terminal perovskite/CuInSe$_2$ tandem solar cells. ACS Nano *14*, 7502–7512.

Kim, D.H., Muzzillo, C.P., Tong, J., Palmstrom, A.F., Larson, B.W., Choi, C., Harvey, S.P., Glynn, S., Whitaker, J.B., Zhang, F., et al. (2019). Bimolecular additives improve wide-band-gap perovskites for efficient tandem solar cells with CIGS. Joule *3*, 1734–1745.

Kinoshita, T., Nonomura, K., Jeon, N.J., Giordano, F., Abate, A., Uchida, S., Kubo, T., Seok, S. Il, Nazeeruddin, M.K., Hagfeldt, A., et al. (2015). Spectral splitting photovoltaics using perovskite and wideband dye-sensitized solar cells. Nat. Commun. *6*, 1–8.

Krückemeier, L., Rau, U., Stolterfoht, M., and Kirchartz, T. (2020). How to report record open-circuit voltages in lead-halide perovskite solar cells. Adv. Energy Mater. *10*, 1902573.

Lin, R., Xiao, K., Qin, Z., Han, Q., Zhang, C., Wei, M., Saidaminov, M.I., Gao, Y., Xu, J., Xiao, M., et al. (2019). Monolithic all-perovskite tandem solar cells with 24.8% efficiency exploiting comproportionation to suppress Sn(ii) oxidation in precursor ink. Nat. Energy *4*, 864–873.

Lu, H., Krishna, A., Zakeeruddin, S.M., Grätzel, M., and Hagfeldt, A. (2020). Compositional and interface engineering of organic-inorganic Lead halide perovskite solar cells. iScience *23*, 1–14.

Meillaud, F., Shah, A., Droz, C., Vallat-Sauvain, E., and Miazza, C. (2006). Efficiency limits for single-junction and tandem solar cells. Sol. Energy Mater. Sol. Cell *90*, 2952–2959.

Nakamura, M., Yamaguchi, K., Kimoto, Y., Yasaki, Y., Kato, T., and Sugimoto, H. (2019). Cd-free Cu(In,Ga)(Se,S)$_2$ thin-film solar cell with record efficiency of 23.35%. IEEE J. Photovoltaics *9*, 1863–1867.

Palmstrom, A.F., Eperon, G.E., Leijtens, T., Prasanna, R., Habisreutinger, S.N., Nemeth, W., Gaulding, E.A., Dunfield, S.P., Reese, M., Nanayakkara, S., et al. (2019). Enabling flexible all-perovskite tandem solar cells. Joule *3*, 2193–2204.

Peters, I.M., Rodriguez Gallegos, C.D., Sofia, S.E., and Buonassisi, T. (2019). The value of efficiency in photovoltaics. Joule *3*, 2732–2747.

Shen, H., Duong, T., Peng, J., Jacobs, D., Wu, N., Gong, J., Wu, Y., Karuturi, S.K., Fu, X., Weber, K., et al. (2018). Mechanically-stacked perovskite/CIGS tandem solar cells with efficiency of 23.9% and reduced oxygen sensitivity. Energy Environ. Sci. *11*, 394–406.

Shockley, W., and Queisser, H.J. (1961). Detailed balance limit of efficiency of p-n junction solar cells. J. Appl. Phys. *32*, 510–519.

Tang, Z., Bessho, T., Awai, F., Kinoshita, T., Maitani, M.M., Jono, R., Murakami, T.N., Wang, H., Kubo, T., Uchida, S., et al. (2017). Hysteresis-free perovskite solar cells made of potassium-doped organometal halide perovskite. Sci. Rep. *7*, 12183.

Tong, J., Song, Z., Kim, D.H., Chen, X., Chen, C., Palmstrom, A.F., Ndione, P.F., Reese, M.O., Dunfield, S.P., Reid, O.G., et al. (2019). Carrier lifetimes of >1 μs in Sn-Pb perovskites enable

efficient all-perovskite tandem solar cells. Science *364*, 475–479.

De Vos, A. (1980). Detailed balance limit of the efficiency of tandem solar cells. J. Phys. D. Appl. Phys. *13*, 839–846.

Uzu, H., Ichikawa, M., Hino, M., Nakano, K., Meguro, T., Hernández, J.L., Kim, H.S., Park, N.G., and Yamamoto, K. (2015). High efficiency solar cells combining a perovskite and a silicon heterojunction solar cells via an optical splitting system. Appl. Phys. Lett. *106*, 013506.

Wang, Z., Zhu, X., Zuo, S., Chen, M., Zhang, C., Wang, C., Ren, X., Yang, Z., Liu, Z., Xu, X., et al.

(2020). 27%-Efficiency four-terminal perovskite/silicon tandem solar cells by sandwiched gold nanomesh. Adv. Funct. Mater. *30*, 1–8.

Xu, J., Boyd, C.C., Yu, Z.J., Palmstrom, A.F., Witter, D.J., Larson, B.W., France, R.M., Werner, J., Harvey, S.P., Wolf, E.J., et al. (2020). Triple-halide wide-band gap perovskites with suppressed phase segregation for efficient tandems. Science *367*, 1097–1104.

Yang, Z., Yu, Z., Wei, H., Xiao, X., Ni, Z., Chen, B., Deng, Y., Habisreutinger, S.N., Chen, X., Wang, K., et al. (2019). Enhancing electron diffusion length in narrow-bandgap perovskites for

efficient monolithic perovskite tandem solar cells. Nat. Commun. *10*, 4498.

Yao, Y., Lv, F., Luo, L., Liao, L., Wang, G., Liu, D., Xu, C., Zhou, G., Zhao, X., and Song, Q. (2020). Highly efficient Sn–Pb perovskite solar cell and high-performance all-perovskite four-terminal tandem solar cell. Sol. RRL *4*, 1900396.

Zhao, D., Wang, C., Song, Z., Yu, Y., Chen, C., Zhao, X., Zhu, K., and Yan, Y. (2018). Four-terminal all-perovskite tandem solar cells achieving power conversion efficiencies exceeding 23%. ACS Energy Lett. *3*, 305–306.

Supplemental Information

Perovskite/CIGS Spectral Splitting

Double Junction Solar Cell with 28%

Power Conversion Efficiency

Motoshi Nakamura, Keishi Tada, Takumi Kinoshita, Takeru Bessho, Chie Nishiyama, Issei Takenaka, Yoshinori Kimoto, Yuta Higashino, Hiroki Sugimoto, and Hiroshi Segawa

SUPPLEMENTAL INFORMATION

Transparent Methods

Materials:
All chemicals were used as-purchased without any purification. Titanium diisopropoxide bis (acetylacetonate) (75 wt.% in isopropanol) and lithium bis (trifluoromethanesulfonyl) imide (LiTFSI) were obtained from Sigma-Aldrich. Bis (trifluoromethanesulfonyl) imide ($Mg(TFSI)_2$) and 4-tert-butylpyridine (tBP) were purchased from Tokyo Chemical Industry (TCI) Co., LTD. 24-nm TiO_2 paste (PST-24NR) was purchased from JGC C&C®. The materials for the perovskite absorber preparation, including $PbBr_2$ (99%), KI (>99.5%), and Magnesium(II) were also obtained from TCI Co., LTD FAI (>99%). MABr (>98%) was purchased from GreatCell Solar Limited, and PbI_2 (99.99%) was purchased from Kojundo Chemical Laboratory Co., LTD. Spiro-OMeTAD (>99.97%) was purchased from Nippon Fine Chemical Co., LTD. Solvents were purchased from Wako Pure Chemical Industries, LTD and Sigma-Aldrich Co. LLC. Mo target (>99.9%), Cu-Ga target (>99.99%), and In target (>99.99%) were obtained from PLANSEE Japan Ltd., Mitsubishi Materials Corporation, and JX Nippon Mining & Metals Corporation, respectively. H_2Se and H_2S gases were purchased from Tomoe Shokai Co., Ltd.

Perovskite Solar Cell Fabrication:
FTO glass with an anti-reflective coating from GEOMATEC Co., Ltd. was employed as a transparent conductive substrate. The substrate was ultrasonically cleaned with acetone and methanol sequentially, and UV-Ozone cleaning was performed for the FTO surface. The compact TiO_2 (c-TiO_2) layer, mesoporous TiO_2 (m-TiO_2) layer, PVK layer, Spiro-OMeTAD layer, and Au layer were sequentially deposited. More specifically, the c-TiO_2 layer was deposited by a spray pyrolysis method from a titanium diisopropoxide bis (acetylacetonate) precursor solution containing LiTFSI and $Mg(TFSI)_2$ in dehydrated ethanol. The m-TiO_2 layer was formed by the spin coating method with a diluted PST-24NR in dehydrated ethanol suspension followed by the Li-doping with LiTFSI containing solution (0.1 M) in acetonitrile. The perovskite precursor solution containing 1.15 M PbI_2, 0.20 M $PbBr_2$, 0.20 M MABr, and 1.09 M FAI was prepared by dissolving all the powders in DMF and DMSO mixed solvent with a volume ratio of 4:1, and separately prepared 0.05 M KI in DMSO was added to the previous solution. The PVK layer was formed via an anti-solvent method with chlorobenzene. Then, LiTFSI and tBP doped Spiro-OMeTAD (60 mM) was spin-casted as the hole transport layer followed by 80 nm-thick Au electrode deposition by thermal evaporation.

CIGS Solar Cell Fabrication:
A cleaned glass substrate was placed in an in-line DC-magnetron sputtering system, where a Mo back electrode and CuGa/In metal precursor with a certain amount of additives such as Na were sequentially deposited. Then, the substrates were placed in a rapid thermal annealing (RTP) furnace for the sulfurization after selenization (SAS) process, where the precursor layers turned into CIGS absorber layers. CIGS absorber layers with various E_g were prepared by tuning some of the SAS process parameters such as temperature. The absorber layers then underwent the Cs treatment for the surface passivation. $Zn(O,S,OH)_x$/ $Zn_{0.8}Mg_{0.2}O$ double layers deposited by a combination of chemical bath deposition and atomic layer deposition techniques were used as the buffer layer. Next, ZnO:B was deposited as a transparent conductive layer by a metal-organic chemical-vapor deposition. Finally, 20 µm of Al and 120 nm of MgF_2 were deposited as the grid electrode and anti-reflective layer, respectively, using the electron beam evaporation method.

Device Characterization:
The current density–voltage (*J–V*) characteristics of the cells were measured with a class AAA solar simulator, WXS-350S-L2MS (Wacom) under the standard test conditions (AM1.5G, 1000 W/m^2, 25 °C). Light intensity was calculated using a Si photodiode, BS-500BK (Bunkokeiki). EQE values were measured with a YQ-M11 instrument (Bunkoukeiki). Dichroic mirrors from Semrock® were used as the spectrum splitter.
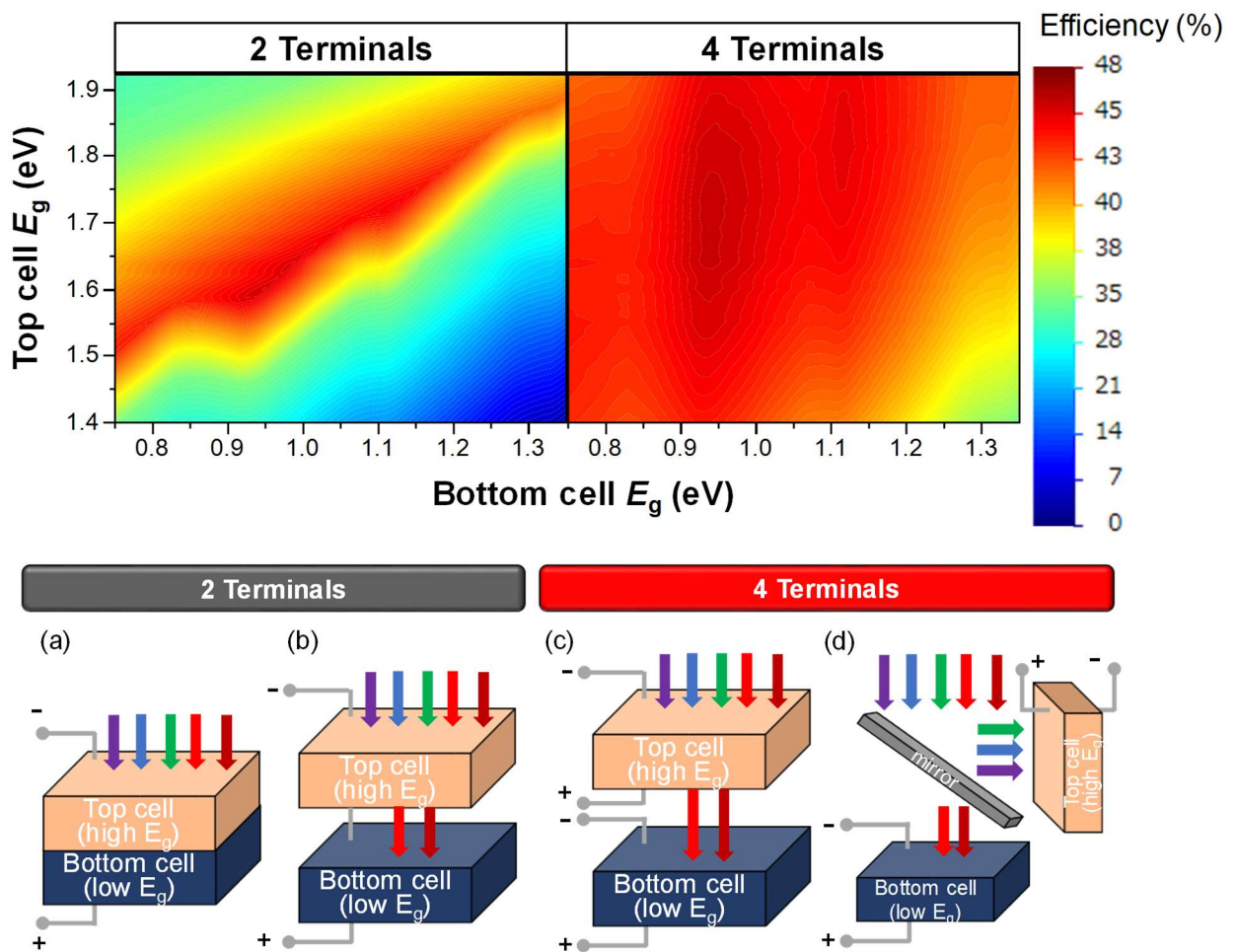
Figure S1. Calculated theoretical efficiency limit of 2 terminal (2-T) and 4 terminal (4-T) double junction solar cells plotted as a function of top and bottom cell bandgaps and schematics of different terminal architectures of the devices: (a) 2-T monolithic, (b) 2-T mechanical stack, (c) 4-T mechanical stack, and (d) 4-T spectrum splitting. The calculation is based on the detailed balance theory (Shockley et al., 1961) and an assumption that every single photons with lower energy than top cell E_g reaches the bottom cell. Related to Figure 1.
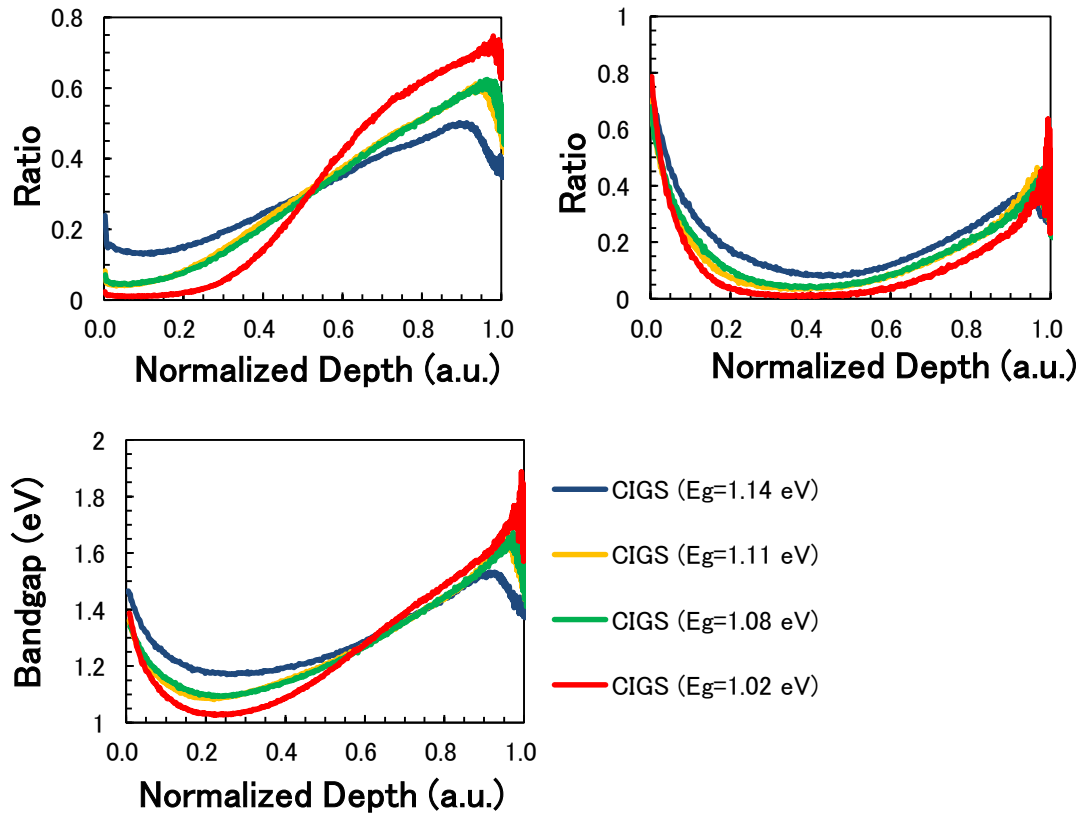
Figure S2. Elemental and E_g Depth profiles of CIGS absorbers used in this report: (a) [Ga]/([Ga]+[In]), (b) [S]/([S]+[Se]), (c) E_g. Related to Figure 2.
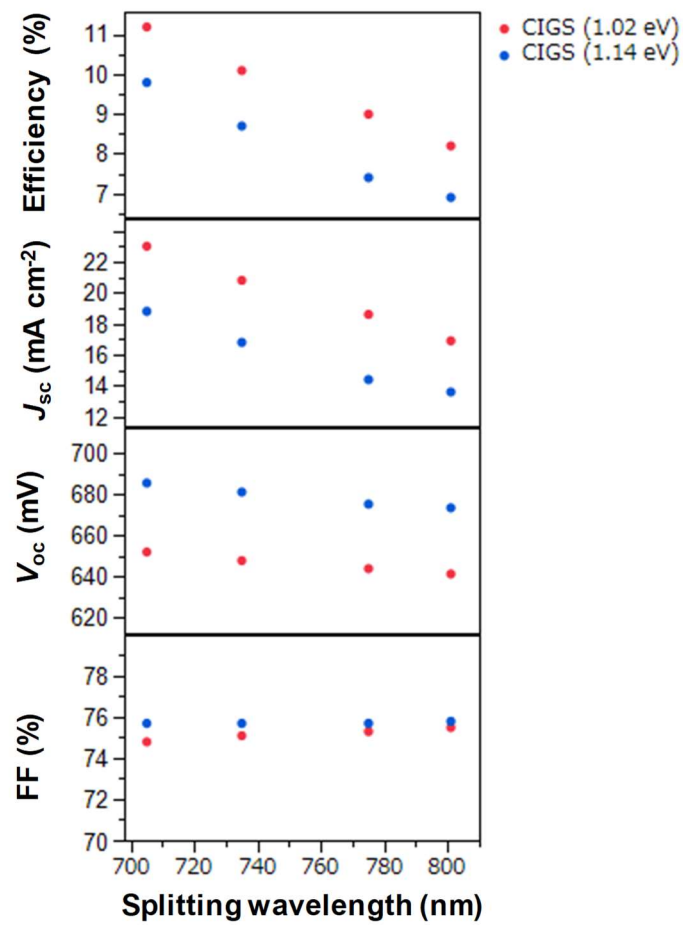
Figure S3. Relation between the solar cell device parameters of CIGS bottom cell with different bandgaps (1.02 and 1.14 eV) as a function of the splitting wavelength of the dichroic mirror. Related to Figure 3.

Table S1. Reported high PCE of perovskite-based double junction solar cells in order of the area by bottom cell distinction. One square centimeter devices are shown in a bold-face. Related to Table 2.

Article	Tandem Architecture	Top cell	Bottom cell	Area (cm^2)	PCE (%)
Chen et al., 2020	4-T mechanical	[Cs,FA,MA]Pb[I,Br]$_3$	Si	0.05	28.6
Uzu et al., 2015	4-T splitting	MAPbI$_3$	Si	0.20	28.0
Duong et al., 2020	4-T mechanical	[Rb,Cs,FA,MA]Pb[I,Br]$_3$	Si	0.21	27.7
Xu et al., 2020	2-T monolithic	[Cs,FA,MA]Pb[I,Br,Cl]$_3$	Si	1.00	27.1
Jaysankar et al., 2019a	4-T mechanical	[Cs,FA]Pb[I,Br]$_3$	Si	0.13	27.1
Wang et al., 2020	4-T mechanical	MAPbI$_3$	Si	0.10	27.0
This work	**4-T splitting**	**[K,FA,MA]Pb[I,Br]$_3$**	**CIGS**	**1.00**	**28.0**
Kim et al., 2019	4-T mechanical	[Cs,FA,MA]Pb[I,Br]$_3$	CIGS	0.06	25.9
Gharibzadeh et al., 2020	4-T mechanical	[Cs,FA]Pb[I,Br]$_3$	CIGS	0.11	25.0
Shen et al., 2018	4-T mechanical	[K,Cs,FA,MA]Pb[I,Br,Cl]$_3$	CIGS	0.30	24.6
Jiang et al., 2020	4-T mechanical	[RbCsFAMA]Pb[I,Br]$_3$	CIGS	0.30	23.9
Jaysankar et al., 2019b	4-T mechanical	[Cs,FA]Pb[I,Br]$_3$	CIGS	0.13	23.8
Al-Ashouri et al., 2019	2-T monolithic	[Cs,FA,MA]Pb[I,Br]$_3$	CIGS	1.00	23.3
Han et al., 2018	2-T monolithic	[Cs,FA,MA]Pb[I,Br]$_3$	CIGS	0.04	22.4
Tong et al., 2019	4-T mechanical	[Cs,FA,MA]Pb[I,Br]$_3$	PVK	0.11	25.0
Lin et al., 2019	2-T monolithic	[Cs,FA]Pb[I,Br]$_3$	PVK	0.05	24.8
Palmstrom et al., 2019	4-T splitting	MAPb[I,Cl]$_3$	PVK	0.06	23.3
Zhao et al., 2018	4-T mechanical	[Cs,FA]Pb[I,Br]$_3$	PVK	0.1	23.1
Yao et al., 2020	2-T monolithic	[Cs,FA,MA]Pb[I,Br]$_3$	PVK	0.06	23.1
Abdollahi et al., 2020	4-T mechanical	[Cs,FA,MA]Pb[I,Br]$_3$	PVK	0.11	23.0
Yang et al., 2019	2-T monolithic	[Cs,FA]Pb[I,Br]$_3$	PVK	0.08	23.0
Kinoshita et al., 2015	4-T splitting	[FA,MA]Pb[I,Br]$_3$	DS	0.16	21.5

References

Shockley, W., and Queisser, H.J. (1961). Detailed Balance Limit of Efficiency of p‑n Junction Solar Cells. J. Appl. Phys. 32, 510‑519.